ELSEVIER

J. Non-Newtonian Fluid Mech. 142 (2007) 199–206

Journal of Non-Newtonian Fluid Mechanics

www.elsevier.com/locate/jnnfm

On the early breakdown of semisolid suspensions

Andreas N. Alexandrou [a,*], Georgios Georgiou [b]

[a] *Mechanical and Manufacturing Engineering Department, University of Cyprus, PO Box 20537, 1678 Nicosia, Cyprus*
[b] *Department of Mathematics and Statistics, University of Cyprus, PO Box 20537, 1678 Nicosia, Cyprus*

Received 28 February 2006; received in revised form 9 August 2006; accepted 18 September 2006

Abstract

Semisolid materials are suspensions of metal alloys which are processed while in a mushy state. In this state, the suspensions behave as viscoplastic materials with time-dependent material properties. During processing, the material is injected at high speed into a mold cavity with the process lasting only fractions of a second. The short-term transient material response is thus very important for the understanding of the rheology and the further development of the process.

A theory based on the Herschel–Bulkley flow model appropriate for the short-term breakage of welded bonds in semisolid metal slurries is proposed. The "strength" of the slurry due to these bonds is assumed to be a function of a coherency parameter which is proportional to the number of welded bonds that break during the application of shear. The evolution of this parameter is described by a first-order kinetics. Using a novel and simple computational method, well suited for free and moving-boundary problems, we study the flow between two coaxial cylinders and obtain accurate results for the evolution of the structure, the extent of the yielded domain and the evolution of the stress. The results and conclusions apply directly to the design and analysis of rotational rheometer experiments for semisolid metal slurries and suspension systems exhibiting similar behavior.

Keywords: Coherency parameter; Thixotropy; Semisolid metals; Herschel–Bulkley fluids; Yield stress; Structural parameter

1. Introduction

Semisolid metal (SSM) alloys are processed in a state between that of a pure solid and a pure liquid. Prior to processing the raw material is melted and allowed to cool and solidify. During solidification, dendrites are broken by mechanical or electromagnetic means. The resultant slurry has an equiaxed microstructure made up of round, rosette-like crystals mixed in eutectic liquid. The specially prepared material is injected into a die (rheocasting) or solidified in billet form for later processing (thixoforming).

The advantages of semisolid processing derive from the fact that, as a solid the material maintains its structural integrity, and as a liquid it flows with relative ease [1,2]. These advantages include low porosity, reduced oxide entrapment, and a lower operating temperature than that of casting in the liquid state [1,2]. The process is used to produce components with complicated form and with close dimensional tolerances reducing the need for further mechanical machining.

Despite its attractive features semisolid processing is hampered by technical problems primarily due to the complex rheology of the material. The effect of the process variables on the filling of dies and the final quality of the parts is not well understood and, therefore, it is difficult to control or optimize the process.

In this work we present a theory appropriate for the short-term breakdown of the continuous solid skeleton of SSM suspensions in conjunction with the flow between two concentring cylinders. This is a typical viscometric flow used in rotational rheometer experiments. The results and conclusions of the present work will apply directly to such experiments. Using a novel computational method suited for problems with free and moving boundaries with singularities, we study the evolution of the strength of the slurry, the extent of the yielded domain and the evolution of the stress at the rotating surface.

In Section 2, we discuss the main issues associated with the fundamental rheology of SSM slurries. In Section 3, we present a general thixotropic theoretical framework which works reasonably well for the long-term description of the slurries [3]. In Section 4, we propose a model for the short-term response of SSM suspensions. This is used in Section 5 to study the structural breakdown of SSM suspension flow between two coaxial

* Corresponding author. Tel.: +357 22892256; fax: +357 22892254.
E-mail address: andalexa@ucy.ac.cy (A.N. Alexandrou).

0377-0257/$ – see front matter © 2006 Elsevier B.V. All rights reserved.
doi:10.1016/j.jnnfm.2006.09.003

cylinders similar to the flow in a rotating rheometer. The numerical results are presented and discussed in Section 6. The paper concludes in Section 7 with the final remarks.

2. Rheological behavior of SSM suspensions

In the mushy state, a semisolid metal is a dense suspension consisting of liquid metal and solid particles the majority of which are welded together due to thermal diffusion to form a continuous solid network.

There are two possible mechanisms relevant to the time-dependent behavior of SSM [4–6]. The first mechanism is the breakdown of the solid structure which involves the breaking up of the bonds between particles due to shear forces. This mechanism occurs during the early stages of the shearing history and is responsible for the rapid decrease in the effective viscosity of the material [4,7,8]. Since in an actual process the breakdown of the structure is the most important effect this mechanism is the focus of the current work.

The second mechanism is the build-up of the solid structure and refers to the formation of metallurgical bonds (necks) between particles, occurring while the sample is at rest [7,8]. Obviously, given the speed of the process relative to thermal diffusion the structure breaks down at a rate much faster than the rate it builds up.

One of the most commonly used methods to study the rheology of SSM slurries is the rotating vane-cup rheometer, with which time-dependent rheological data can be obtained following the sudden application of a constant rotational speed. The shear stress (and thus the apparent viscosity) is determined as a function of time by measuring the torque on the rotational part of the rheometer [4–9]. Typical time-dependent results obtained in our experiments are shown in Fig. 1. In general, it has been found that for a given rotational speed the shear stress (or the viscosity) decreases rapidly at the start of shearing before it approaches a steady value. The rate at which the viscosity decreases is a strong function of the rotational speed and the solid volume fraction of the sample [4–9].

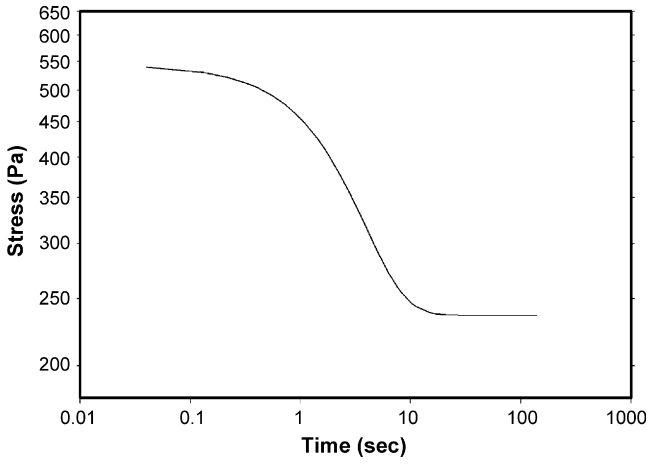

Fig. 1. Typical experimental results for the variation of the stress with time for SSM slurry from a rotational experiment [9].

Notwithstanding the experimental difficulties, the different experimental techniques used for material characterization and the wide variance in the conditions used, it is generally accepted that semisolid slurries behave as viscoplastic materials with a finite yield stress and time-dependent material properties. In the SSM scientific community there is wide consensus that the slurries can be represented well using the Herschel–Bulkley model [3,10,13–17]. Currently the short-term response of SSM slurries is not well modeled and more accurate models are needed for the early stages of the deformation. Therefore, the objective here is to expand the theory based on the Herschel–Bulkley model by including the early breakdown of the solid structure.

3. General thixotropic model for SSM suspensions

In this section, we discuss a general theoretical framework applicable to many suspension systems. The framework provides a convenient basis on which to develop the breakdown model proposed here.

In a previous work, Burgos et al. [3] used a structural-parameter model, similar to those in Refs. [12,13] to describe the thixotropy of SSM slurries. The structural parameter, ξ, characterizes the state of the structure. In a fully structured state, i.e. when all the particles are connected, ξ is assumed to be unity. In a fully broken state, when no particles are connected, ξ is assumed to be zero, as illustrated in Fig. 2.

The evolution of the structural parameter is governed by a first-order rate equation, similar to those used to describe chemical reaction kinetics [18]. It is assumed that the rate of breakdown depends on both the fraction of links existing at any instant and the deformation rate. Similarly, the rate of build-up is assumed to be proportional to the fraction of links remained to be formed

$$\frac{\mathrm{D}\xi}{\mathrm{D}t} = \alpha_0(1-\xi) - \alpha_1\xi\dot{\gamma}\,\mathrm{e}^{\alpha_2\dot{\gamma}} \tag{1}$$

where $\mathrm{D}\cdot/\mathrm{D}t$ is the material derivative, the recovery parameter, α_0, and the breakdown parameters, α_1 and α_2, are empirical constants to be determined experimentally, and $\dot{\gamma}$ is the second invariant of the rate of strain tensor, $\mathbf{D} = \nabla\mathbf{u} + (\nabla\mathbf{u})^{\mathrm{T}}$. The exponential dependence on the deformation rate, in the rate of breakdown term of Eq. (1), is included in order to account for the fact that the shear stress evolution in the shear-rate step-up experiment is faster than that in the step-down case [10,11].

At equilibrium, the rates of breakdown and recovery are equal. For constant $\dot{\gamma}$, the equilibrium value of the structural

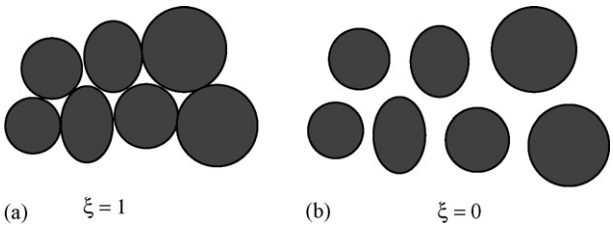

Fig. 2. Coherency parameter in a (a) fully structured state and (b) fully broken state.

parameter, ξ_e, is then obtained from Eq. (1) as

$$\xi_e = \frac{1}{1 + (\alpha_1/\alpha_0)\dot{\gamma}\, e^{\alpha_2 \dot{\gamma}}} \tag{2}$$

Consistent with experimental observations the suspension is assumed to behave as a Herschel–Bulkley fluid. The model is a combination of the Bingham and power-law fluid models. For SSM slurries the Bingham fluid model accounts for the presence of a finite yield stress, while the power-law model accounts for the shear-dependency of the suspension. Here, the material parameters of the model are assumed to be functions of both the solid fraction and the structural parameter:

$$\boldsymbol{\tau} = \left[\frac{\tau_y(s,\xi)}{\dot{\gamma}} + K(s,\xi)\dot{\gamma}^{n(s,\xi)-1}\right]\mathbf{D} \tag{3}$$

where $\boldsymbol{\tau}$ is the viscous stress tensor, $K(s, \lambda)$ the consistency index, $n(s, \lambda)$ the power-law index, and $\tau_y(s, \lambda)$ is the yield stress. In a simple shear flow experiment, Eq. (3) reduces to

$$\tau = \tau_y(s,\xi) + K(s,\xi)\dot{\gamma}^{n(s,\xi)} \tag{4}$$

The material parameters in the model, α_0, α_1 and α_2, and the material functions, $K(s, \xi)$, $n(s, \xi)$ and $\tau_y(s, \xi)$, are identified using appropriate experimental data.

4. Short-term breakdown of SSM suspensions

The thixotropic model described in Section 3 was applied to the experiments performed by Modigell et al. [13] in order to determine material constants for SSM suspensions [3]. The results of this work have shown that with proper choice of material constants the model could predict fairly well long-term step-up and step-down experiments. The Herschel–Bulkley model that captured well the long-term behavior supported the presence of a residual yield stress even after several minutes of shearing. Note that the experiments were lengthy, lasting for several minutes a time frame much longer than any real SSM process. Unlike the long-term behavior, the short-term response of the slurry immediately after the initial application of shear was not predicted well. This implies that the physics of the early breakdown is different from that of the long-term behavior.

Recent experiments by Salvo et al. [19] showed that the solid matrix formed by the bonding of solid particles is quite extensive. Three-dimensional X-ray micro-tomography revealed that solid particles formed a very coherent three-dimensional structure (a fact consistent with the presence of a finite yield stress). The physics of the early breakdown are indeed related to this initial structure and its subsequent breakdown upon the application of shear. Obviously, once it breaks down, the structure cannot recover in the short time of the process. Therefore, shear strain step-up/step-down experiments such as the one used in [13] are not useful in describing the short-term response. More useful information for understanding the behavior of SSM slurries may be provided by detailed stress versus time data obtained from rotational experiments.

In line with the above observations we developed a model for the short-term response based on the following principles:

1. The bulk of the finite yield stress of SSM slurries is primarily due to the welded bonds between solid particles. Their effect is defined as the "strength" of the slurry τ_0. This is a time dependent contribution to the rheology of SSM slurries. The breakage of bonds due to shear explains the characteristic rapid decrease in the stress observed in transient experiments.
2. In the short time of the process we assume that the contribution of the structure evolution as described earlier with the parameter ξ is a second-order effect. Possible particle–particle and fluid–particle interactions due to the evolution of the structure (and the part of the solid skeleton that survives the shearing) are included in a time-invariant but rate of strain-dependent contribution, τ_{ss}. Note that a more complicated model will also include for the same time scale the evolution of the structure as explained in Section 3. In such a case the number of unknown parameters increases significantly and the model becomes less practical to use. Moreover, it becomes almost impossible to verify experimentally the validity of such complex model.

Based on the above assumptions and physical observations and by defining a coherency parameter λ that represents the relative number of welded bonds that eventually break ($\lambda > 0$, at steady state) we can write

$$\tau = \tau_0(s, \lambda(t)) + \tau_{ss}(s, \dot{\gamma}_e, \dot{\gamma})$$

where

$$\tau_{ss}(s, \dot{\gamma}, \dot{\gamma}_e) = \tau_e(s, \dot{\gamma}_e) + \tau_{pp}(s, \dot{\gamma}) + \tau_{fp}(s, \dot{\gamma})$$

with $\tau_{pp}(s, \dot{\gamma})$ being the particle–particle and $\tau_{fp}(s, \dot{\gamma})$ the fluid–particle interactions taken to be functions of $\dot{\gamma}$. The term $\tau_e(s, \dot{\gamma}_e)$ is the part of the solid network that survives the shearing at a given steady-state $\dot{\gamma}_e$.

Experimental data and the consensus in SSM modeling indicate that $\tau_{ss}(s, \dot{\gamma}, \dot{\gamma}_e)$ fits very well a Herschel–Bulkley fluid model [9]. Therefore

$$\tau = \underbrace{\tau_0(s, \tau(\lambda))}_{\text{sturry strength}} + \underbrace{\tau_s(s, \dot{\gamma}_e) + K(s, \dot{\gamma}_e)\dot{\gamma}^{n(s,\dot{\gamma}_e)}}_{\text{"steady state"}} \tag{5}$$

The functions $\tau_s(s, \dot{\gamma}_e)$, $K(s, \dot{\gamma}_e)$ and $n(s, \dot{\gamma}_e)$ are obtained by curve-fitting experimental data. These are steady-state data points from stress versus time measurements obtained after long shearing time when the flow reaches steady state where $\dot{\gamma} = \dot{\gamma}_e$. It is important to note here that the error in estimating the parameters may become quite large, if the true rate of strain is not used in the analysis. Unfortunately, this is the case in the majority of published works on the rheology of SSM.

The time-dependent function $\tau_0(s, \lambda(t))$ must be defined *a priori*. The simplest, and most obvious approach is to assume a linear dependence of the form:

$$\tau_0(s, \lambda(t)) = \lambda(t)\tau_0(s)$$

To complete the theoretical formulation we also need to specify the dependence of the coherency parameter on the local flow conditions. The evolution of λ is assumed to follow an expression similar to the one used in Section 3 for the evolution of

the structure of the slurry. Since the rate of build-up during the early stages of deformation is insignificant, $\alpha_0 = 0$ and hence the expression can be written as

$$\frac{D\lambda}{Dt} = -\alpha_1 \lambda \dot{\gamma}\, e^{\alpha_2 \dot{\gamma}} \tag{6}$$

5. Flow between coaxial cylinders

The objective of the present work is to study the breakdown of the solid structure in SSM slurries in conjunction with the flow between two coaxial cylinders. This is a prototype flow used in rotational rheometers in order to determine material properties. The results and conclusions apply directly to the design of such experiments and to the subsequent analysis of the data. Fig. 3 shows the schematic of the flow near the rotating cylinder.

Here we will assume that due to the short time of interest, thermal diffusion is limited and hence the temperature T and the solid volume fraction $s(T)$ of the slurry remain constant. Consequently the dependence on s in the following analysis will be ignored. In case thermal effects are important the energy equation with a suitable model for the solid fraction dependence must be introduced.

The conservation of linear momentum for the flow geometry given in Fig. 3 is given by

$$\rho \frac{\partial u}{\partial t} = \frac{1}{r^2}\frac{\partial}{\partial r}(r^2 \tau) \tag{7}$$

where u is the angular velocity, $\tau = \tau_{r\theta}$, and ρ is the density. From Eq. (5), we get

$$\tau = \lambda \tau_0 + \tau_s + K\dot{\gamma}^n \tag{8}$$

where $\dot{\gamma} = |r(\mathrm{d}/\mathrm{d}r)(u/r)|$. The inner cylinder is assumed to rotate at a rate ω, and thus $u(R_1) = \omega R_1 = U$. In the unyielded region, i.e. $r_{max} < r < R_2$ where R_2 is the radius of the outer cylinder it is assumed that the material is stagnant, i.e. $u(r > r_{max}) = 0$. Initially the flow is assumed to be at rest. As discussed below, due to the special method of solution used here the computational domain includes only the yielded part of the domain as shown in Fig. 4.

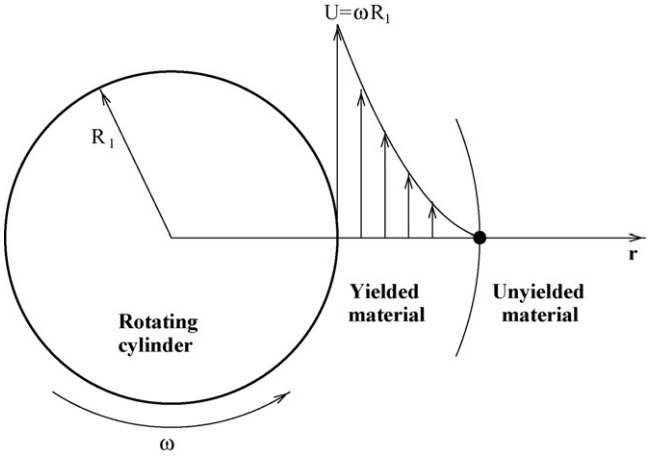

Fig. 3. Schematic of the flow geometry. Due to the motion of the cylinder the adjacent material yields while away from the cylinder the material remains unyielded.

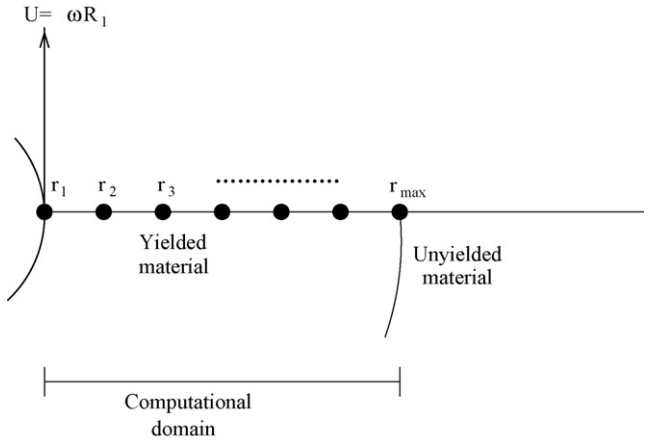

Fig. 4. Schematic explaining the method of solution: the velocity distribution is fixed and the solution procedure seeks to find the location of the nodes that have been assigned a particular velocity, i.e. unknowns are the coordinates (r_i) of the nodes. Note that the location of the last node r_{max} is by default the length of the yielded domain.

For this simple shear flow experiment, the evolution of the coherency parameter (Eq. (6)) reduces to

$$\frac{\partial \lambda}{\partial t} = -\alpha_1 \lambda \dot{\gamma}\, e^{\alpha_2 \dot{\gamma}} \tag{9}$$

By using R_1, U, and $K(U/R_1)^{(n-1)}$ as scales, respectively, for length, velocity, and viscosity, we obtain the following dimensionless forms of Eqs. (7)–(9):

$$Re \frac{\partial u}{\partial t} = \frac{1}{r^2}\frac{\partial}{\partial r}(r^2 \tau) \tag{10}$$

$$\tau = \lambda B_1 + B_2 + \dot{\gamma}^n \tag{11}$$

$$\frac{\partial \lambda}{\partial t} = -\alpha_1' \lambda \dot{\gamma}\, e^{\alpha_2' \dot{\gamma}} \tag{12}$$

where all variables are dimensionless including the constants α_1' and α_2' (the primes will be dropped from hereafter). The generalized Reynolds number, Re, and the Bingham numbers, B_1 and B_2, are given by

$$Re = \frac{\rho U R_1}{K}\frac{R_1^{(n-1)}}{U^{(n-1)}}, \qquad B_1 = \frac{\tau_0}{K}\frac{R_1^n}{U^n}, \qquad B_2 = \frac{\tau_s}{K}\frac{R_1^n}{U^n}$$

5.1. Method of solution

Because Herschel–Bulkley models are singular, finding an analytical solution is possible only for very simple, steady, and mostly unidirectional flows. In time-dependent and more geometrically complex flows, the ideal Herschel–Bulkley model is typically regularized in order to remove the singularity and improve computational efficiency. One of the most popular regularizations is the one introduced by Papanastasiou [20], which uses a smooth exponential function to represent a steep rise in the stress in the limit of zero shear rate. With proper use of the regularization parameter this model can predict with fidelity the flow and stress fields along with the location of the yielded and unyielded surfaces [3].

Since regularized Herschel–Bulkley models are viscous approximations of the ideal model, in a strictly mathematical sense, they can never reproduce exactly the ideal behavior. The ultimate objective, however, of the present work is to apply the results to the design of rotational-rheometer experiments and in the proper analysis of the data presumably through a reverse-engineering approach. It is important then to get results free of any ambiguity in terms of their accuracy.

Fortunately, the flow geometry allows the use of the inverse finite element method (IFEM) solution procedure [21]. As we will elaborate below this is an "inverse" solution procedure where the dependent variable (for example the velocity) is fixed and without inverting the equations the solution is obtained for the independent variable such as the location of the computational nodes. In simpler terms, the procedure seeks to find the location of the nodes which correspond to a predefined velocity distribution (Fig. 4).

The discretization of the conservation of linear momentum (Eq. (10)) follows a classical Galerkin finite element approach using three-noded line elements:

$$R(\mathbf{r}_i) = \int_0^{r_{\max}} \phi_i \left[Re \frac{\partial u}{\partial t} - \frac{1}{r^2}\frac{\partial}{\partial r}(r^2\tau) \right] 2\pi r \, \mathrm{d}r = 0 \tag{13}$$

It is obvious that in this case the mesh is not fixed but moves with velocity $u_\mathrm{m} = (\mathrm{d}r_i/\mathrm{d}t)$. Therefore

$$\frac{\partial u}{\partial t} = \frac{\partial u}{\partial t} - u_\mathrm{m}\frac{\partial u}{\partial r}$$

where $(\mathrm{d}u/\mathrm{d}t)$ is a total derivative, i.e. is the rate of change of the velocity at a node.

Following a standard Finite Element formulation and by integrating by parts Eq. (13) reduces to

$$R(\mathbf{r}_i) = \int_0^{r_{\max}} \left[\phi_i Re \left(\frac{\mathrm{d}u}{\mathrm{d}t} - u_\mathrm{m}\frac{\partial u}{\partial r} \right) + \tau \left(\frac{\partial \phi_i}{\partial r} - \frac{\phi_i}{r} \right) \right] r \, \mathrm{d}r - r_{\max}\tau|_{r=r_{\max}} = 0 \tag{14}$$

where $r_{\max}$ is the location of the last node is the limit of the yielded domain. This limit (which is indeed a key parameter) is obtained as a function of time automatically with the solution. The IFEM is implemented by considering the fact that the velocity in the yielded part varies from $u = 1$ at the rotating surface to $u = 0$ at $r = r_{\max}$. The velocity is distributed and kept constant at all times at the computational nodes, hence $(\mathrm{d}u/\mathrm{d}t) = 0$.

The advantages of the IFEM approach for fluids with yield stress are obvious:

(a) since the solution is limited to the yielded part of the material, the singularity is automatically removed, and hence the solution corresponds to the ideal constitutive model without any regularization;
(b) the boundary conditions are applied and satisfied exactly.

The resulting non-linear system of equations is solved using a Newton–Raphson procedure with its quadratic convergence characteristics:

$$\frac{\partial r(\mathbf{r}_i)}{\partial \mathbf{r}_j} \mathrm{d}\mathbf{r}_j = -R(\mathbf{r}_i)$$

Note that the derivatives of the residual equations $R(\mathbf{r}_i)$ are obtained with respect to the unknown nodal locations $\mathbf{r}_j$.

The Jacobian of the Newton–Raphson procedure is saved using an element-by-element storage and solved by an iterative method based on a modification of the biconjugate gradient stabilized method [22,21]. The Jacobi preconditioning was used to speed up convergence. For converged results, usually two to three iterations in the Newton–Raphson procedure are necessary at each time step.

The evolution equation (Eq. (12)) (corrected for the fact that the mesh moves with velocity u_m):

$$\frac{\mathrm{d}\lambda}{\mathrm{d}t} = u_\mathrm{m}\frac{\partial \lambda}{\partial r} - \alpha_1 \lambda \dot{\gamma}\, \mathrm{e}^{\alpha_2 \dot{\gamma}} \tag{15}$$

at each Newton–Raphson iteration step is solved explicitly for each node using high-order finite difference approximation for the velocity gradient, subject to the boundary condition that at the last (extreme) boundary node ($r = r_{\max}$) $\lambda = 1.0$. The solution advances to the next time step when all unknowns converge to the convergence criterion set to a relative error of 10^{-7}.

6. Results

Fig. 5 shows a typical fluid behavior for $Re = 1$, $B_1 = 3$, $B_2 = 1$, $n = 0.5$ and $\alpha_1 = \alpha_2 = 0.01$. The simulation is started with an arbitrarily small yielded domain (i.e. $r = 1 + \epsilon$). For mesh-independent results we used a total of 40 one-dimensional quadratic elements and ϵ was set to 0.01. The time steps used for stable solutions were in the order of 10^{-6}. In all the simulations we assumed that the material between the two cylinders is partially yielded, i.e. $R_2 > r_{\max}$.

Upon application of shear, the yielded domain increases quite rapidly to a quasi-steady-state which is independent of

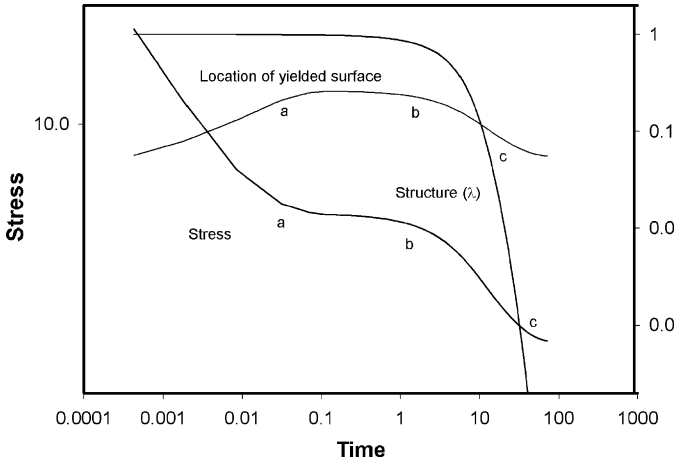

Fig. 5. Typical fluid behavior: upon the application of shear the yielded domain increases rapidly to a quasi-steady-state and then shrinks to a final steady value. During deformation the material breaks down continuously while the stress undergoes a typical sigmoidal variation to a final steady state ($Re = 1$, $B_1 = 3$, $B_2 = 1$, $n = 0.5$, $\alpha_1 = \alpha_2 = 0.01$).

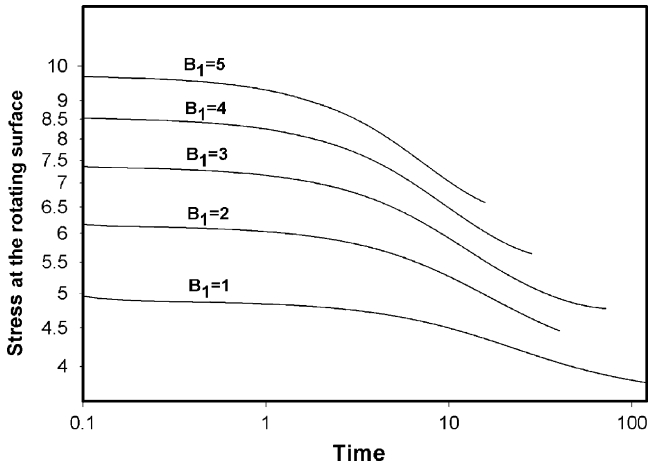

Fig. 6. Effect of B_1 on the stress at the rotating surface ($Re = 1$, $B_1 = 1$–5, $B_2 = 1$, $n = 0.5$, $\alpha_1 = \alpha_2 = 0.01$).

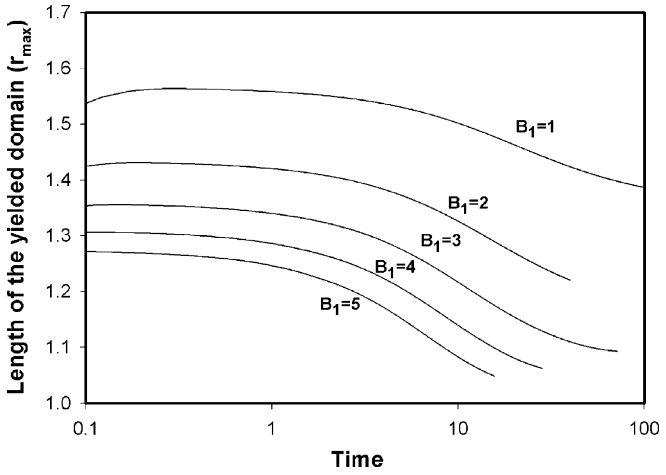

Fig. 7. Effect of B_1 on the length of the yielded domain ($Re = 1$, $B_1 = 1$–5, $B_2 = 1$, $n = 0.5$, $\alpha_1 = \alpha_2 = 0.01$).

the choice of ϵ (point a on the figure) and then after a given time (point b) it starts to shrink to a final steady value (point c). As seen clearly from the figure, during deformation the material breaks down continuously while the stress undergoes a typical sigmoidal variation to a final steady state. This behavior is consistent with actual experimental results as those shown in Fig. 1.

The development of the flow and the various flow parameters are linked to the imposed rate of strain due to the rotation. By approximating the derivatives using the length of the yielded domain Δr we get $\dot{\gamma} = |r(\mathrm{d}/\mathrm{d}r)(u/r)| \approx (U/\Delta r)$. This result shows that the imposed rate of strain and, hence the stress, decrease with increasing Δr. The reverse is also true when Δr decreases. However, due to the continuous breakdown of the structure there is a continuous decrease in the stress. Therefore, the final stress level is the combination of the two, sometimes competing, effects. It is clear that data from rotational experiments for such materials must be analyzed with caution and that proper modeling of the experiment with high fidelity simulations may be necessary.

Below for uniformity we present results for times $t > 0.001$ seconds since our experimental equipment cannot reliably verify the results at shorter time scales. This corresponds to a non-dimensional time of $t = 0.01$. Moreover, the simulations in much shorter times are not reliable because as the flow is started from rest the unavoidable singular flow behavior then is affected by the choice of ϵ and the time step Δt.

Figs. 6–8 document the effects of the initial strength of the slurry as reflected by B_1. As shown quite clearly in the figures, while the stress level at the rotating cylinder increases with B_1 the maximum extent of the yielded domain decreases with B_1. Both results are expected because of the higher strength of the slurry. Given the higher stress for the larger B_1 the rate of breakdown increases with B_1 as shown in Fig. 8.

Figs. 9–11 show the effects of the power-law exponent n. The figures show that at a given time both the stress level at the rotating cylinder and the extent of the yielded domain increase with increasing n. This implies that the increase due to the power exponent overcompensates the stress reduction due to

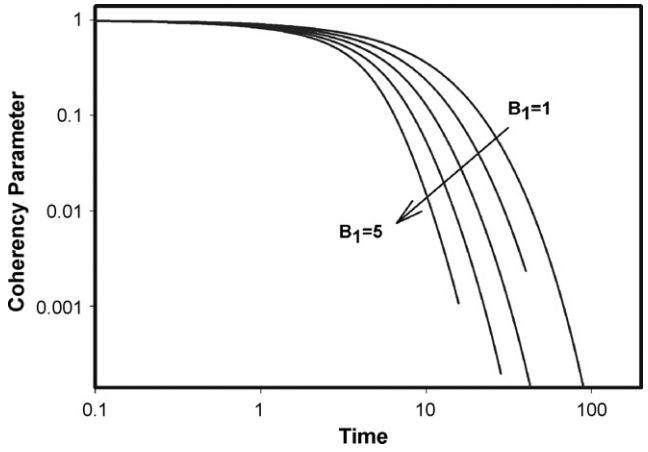

Fig. 8. Effect of B_1 on the coherency parameter λ at the rotating surface ($Re = 1$, $B_1 = 1$–5, $B_2 = 1$, $n = 0.5$, $\alpha_1 = \alpha_2 = 0.01$).

the decrease in the rate of strain that results from the increase in Δr. For the same reason as shown in Fig. 11 the rate of breakdown decreases with increasing n as a result of the decrease in the rate of strain.

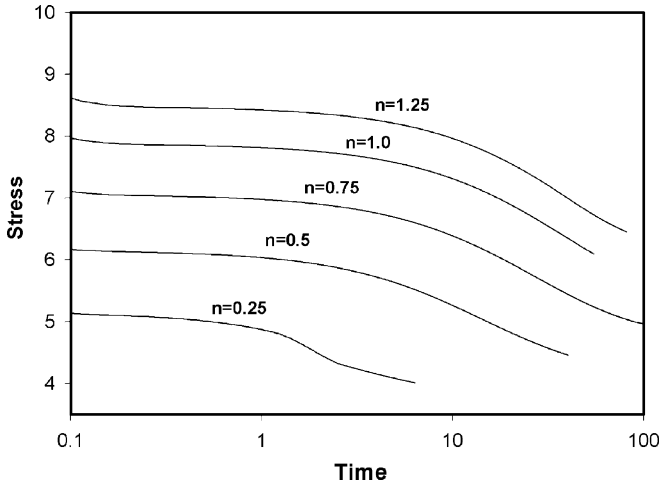

Fig. 9. Effect of n on the stress at the rotating surface ($Re = 1$, $B_1 = 2$, $B_2 = 1$, $n = 0.25$, 0.5, 0.75, 1.0, 1.25, $\alpha_1 = \alpha_2 = 0.01$).

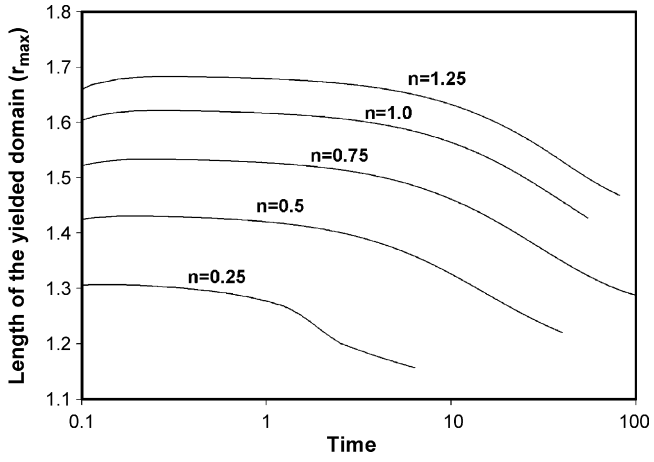

Fig. 10. Effect of n on the length of the yielded domain ($Re = 1$, $B_1 = 2$, $B_2 = 1$, $n = 0.25, 0.5, 0.75, 1.0, 1.25$, $\alpha_1 = \alpha_2 = 0.01$).

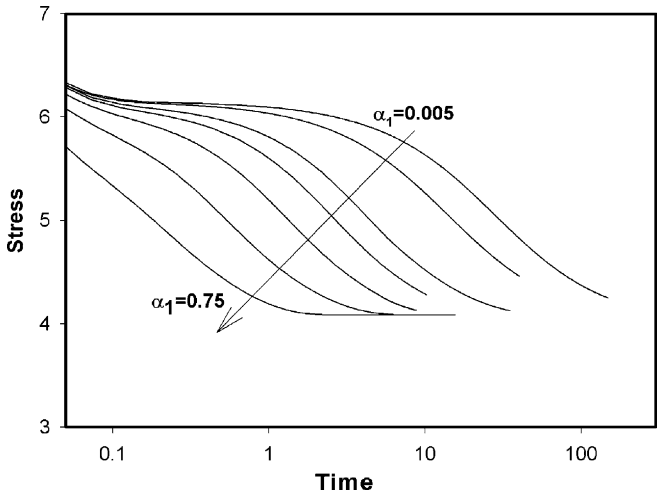

Fig. 12. Effect of α_1 on the stress at the rotating surface ($Re = 1$, $B_1 = 2$, $B_2 = 1$, $n = 0.5$, $\alpha_1 = 0.005, 0.01, 0.03, 0.05, 0.1, 0.25, 0.75$, $\alpha_2 = 0.01$).

Figs. 12–14 demonstrate the effect of the parameter α_1 which controls the rate of breakdown of the structure. The figures show that at a given time both the stress level at the rotating cylinder is higher for smaller values of α_1. This is due to the fact that for a smaller rate of decay at the same time the residual strength of the slurry is high and hence the resultant stress. The higher stress justifies the increased length of the yielded domain with decreasing α_1 as shown in Fig. 13. Finally the rate of breakdown predicted in Fig. 14 is consistent with the definition of the parameter.

The results of the simulation indicate that the flow within the rotational rheometer is not only a strong function of time but it is also quite complex. The details of the flow and the internal structure of the slurry depends on factors such as the material constants and their evolution and on hydrodynamic effects within the rheometer and the evolution of the yielded and unyielded domains. This complexity raises concerns about the routine use of rotational rheometers as a standard method to determine transient material constants for SSM slurries. Reliable data can only be extracted by an effective use of computational

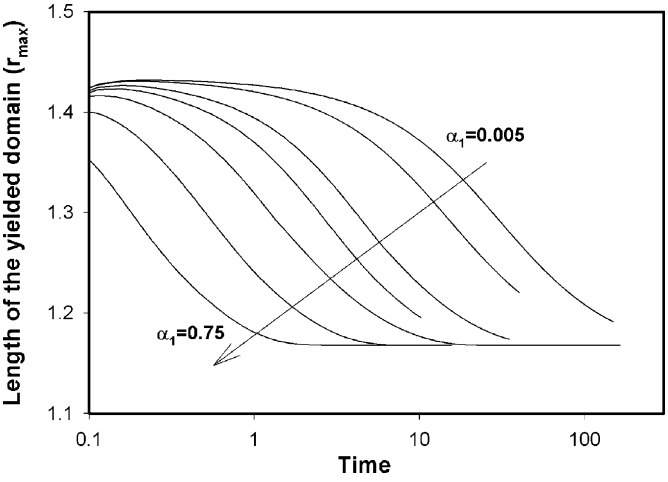

Fig. 13. Effect of α_1 on the length of the yielded domain ($Re = 1$, $B_1 = 2$, $B_2 = 1$, $n = 0.5$, $\alpha_1 = 0.005, 0.01, 0.03, 0.05, 0.1, 0.25, 0.75$, $\alpha_2 = 0.01$).

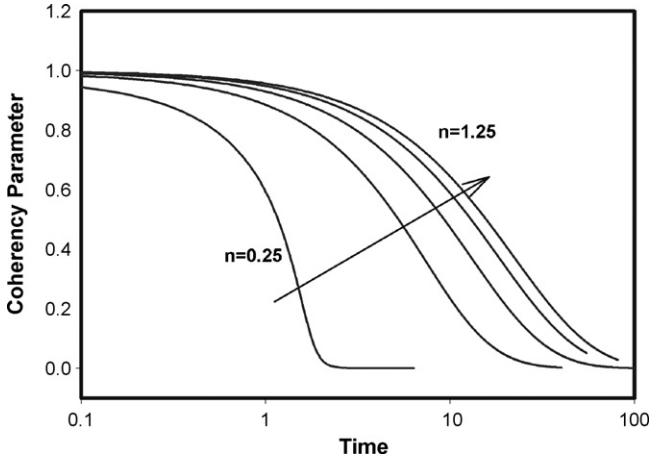

Fig. 11. Effect of n on the coherency parameter λ at the rotating surface ($Re = 1$, $B_1 = 2$, $B_2 = 1$, $n = 0.25, 0.5, 0.75, 1.0, 1.25$, $\alpha_1 = \alpha_2 = 0.01$).

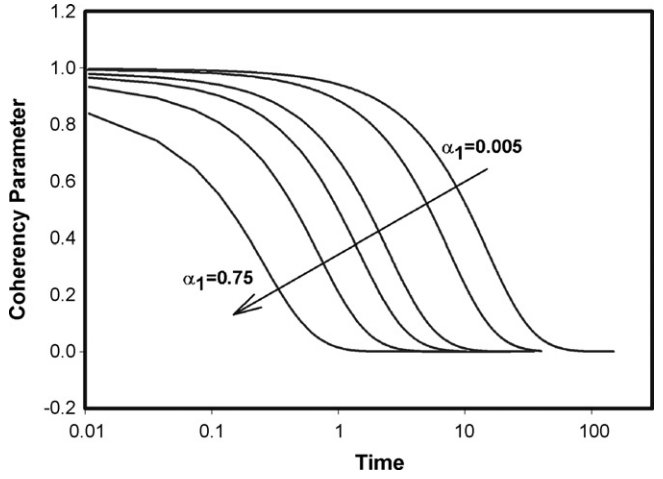

Fig. 14. Effect of α_1 on the coherency parameter λ at the rotating surface ($Re = 1$, $B_1 = 2$, $B_2 = 1$, $n = 0.5$, $\alpha_1 = 0.005, 0.01, 0.03, 0.05, 0.1, 0.25, 0.75$, $\alpha_2 = 0.01$).

rheology where one makes a combined and parallel use of both the experiments and of high fidelity numerical simulations.

7. Conclusions

The short-term response of semisolid materials in a rotational rheometer is modeled using the Herschel–Bulkley fluid model. The yield stress is decomposed into two parts: one that breaks down during the early stages of the deformation, and the other that survives the shearing after a long time. It is assumed that the first component is a linear function of the coherency parameter and that the other, combined with the consistency and the power-law indices, constitute the Herschel–Bulkley flow behavior observed in steady-state experiments. The evolution of the coherency parameter is defined by a first-order rate equation.

The above discussion shows clearly that the strong time-dependent behavior of semisolid slurries plays a critical role in the flow development of SSM slurries. This highlights the need to use computational rheology as a way to extract true material constants. It is expected then that in a real process the time-dependent behavior will affect the quality of the parts being made using this technology.

References

[1] M.C. Flemings, Behavior of metal alloys in the semisolid state, Metall. Trans. A 22 (1991) 957–981.
[2] D.H. Kirkwood, Semisolid metal processing, Int. Mater. Rev. 39 (5) (1994) 173–189.
[3] G.R. Burgos, A.N. Alexandrou, V.M. Entov, Thixotropic behavior of semisolid slurries, J. Mater. Process. 110 (2001) 164–176.
[4] C.J. Quaak, PhD Thesis, Delft University of Technology, The Netherlands, 1996.
[5] M. Mada, F. Ajersch, Rheological model of semisolid A356-SiC composite alloys. Part I. Dissociation of agglomerate Structures during shear, Mater. Sci. Eng. A 212 (1996) 157–170.
[6] M. Mada, F. Ajersch, Rheological model of semisolid A356-SiC composite alloys. Part II. Reconstitution of agglomerate structures at rest, Mater. Sci. Eng. A 212 (1996) 171–177.
[7] T.Y. Liu, P.J. Ward, D.H. Kirkwood, H.V. Atkinson, Rapid compression of aluminum alloys and its relationship to thixoformability, Metall. Trans. A 34 (2003) 409–417.
[8] M. Modigell, L. Pape, M. Hufschmidt, Kinematics of structural changes in semisolid alloys by shear and oscillation experiments, in: Proceedings of the Eighth International Conference on Semi-Solid Processing of Metals and Alloy, Limassol, Cyprus, September 21–23, 2004.
[9] N. Tonmukayakul, Q.Y. Pan, A.N. Alexandrou, D. Apelian, Transient flow characteristics and properties of semi-solid aluminum alloy A356, in: Proceedings of the Eighth International Conference on Semi-Solid Processing of Metals and Alloys, Limasol, Cyprus, September 21–23, 2004.
[10] M. Mada, F. Ajersch, Thixotropic effects in semi-solid Al–6% Si alloy reinforced with SiC particles, in: R.B. Bhagat, al. et (Eds.), Metal and Ceramic Matrix Composites: Processing Modeling and Mechanical Behavior, The Minerals, Metals & Materials Society, 1990, pp. 337–350.
[11] H. Peng, K.K. Wang, Steady-state and transient rheological behavior of a semi-solid tin–lead alloy in simple shear flow, in: D.H. Kirkwood, P. Kapranos (Eds.), Proceedings of the Fourth International Conference on Semi-Solid Processing of Alloys and Composites, The University of Sheffield, England, 1996, pp. 2–9.
[12] P. Kumar, C.L. Martin, S. Brown, Constitutive modeling and characterization of the flow behavior of semi-solid metal alloy slurries. I. The flow response, Acta Met. Mater. 42 (11) (1994) 3595–3602.
[13] M. Modigell, J. Koke, J. Petera, Time-dependent rheological properties of semisolid metal alloy, Mech. Time-Dependent Mater. 3 (1999) 15–30.
[14] C.L. Martin, P. Kumar, Constitutive modeling and characterization of the flow behavior of semi-solid metal alloy slurries. II. Structural evolution under shear deformation, Acta Met. Mater. 42 (11) (1994) 3603–3614.
[15] A. Ahmed, A.N. Alexandrou, Processing of semi-solid materials using a shear-thickening Bingham fluid model, in: Proceedings of the 1994, ASME Fluids Engineering Division Summer Meeting, FED-vol. 179, ASME, New York, 1994, pp. 83–87.
[16] F. Bardinet, A.N. Alexandrou, W. Loue, Numerical simulation of die filling in semisolid metal processing, in: R. Hughen (Ed.), Light Metals '97, 15086, TMS, Warrendale, PA, 1997, pp. 945–951.
[17] F. Bardinet, A.N. Alexandrou, Thixo-module development for simulator, Pechiney Internal Report, 1998.
[18] F. Moore, The rheology of ceramic slips and bodies, Trans. Br. Ceram. Soc. 58 (1959) 470–494.
[19] L. Salvo, M. Pana, M. Suery, M. DiMichiel, O. Nielsen, D. Bernard, Application of X-ray microtomography to the microstructural characterization of Al–Cu alloys during solidification and partial remelting, in: H. Kaufmann (Ed.), Proceedings of the Second International Light Metals Conference, St. Woolf-gang, Austria, June 8–10, 2005, pp. 209–214.
[20] T.C. Papanastasiou, Flows of materials with yield, J. Rheol. 31 (1987) 385–404.
[21] A.N. Alexandrou, An inverse finite element method for directly formulated free boundary problems, Int. J. Numer. Meth. Eng. 28 (1989) 2383–2396.
[22] H. Van Der Vorst, Bi-CGSTAB: A fast and smoothly converging variant of Bi-CG for the solution of nonsymmetric linear systems, SIAM J. Sci. Stat. Comput. 13 (1992) 631–644.